Batteries & Supercaps

Research Article
doi.org/10.1002/batt.202400737

Chemistry Europe
European Chemical Societies Publishing

www.batteries-supercaps.org

New Non-Invasive Method to Monitor and Reverse Faradaic Imbalance in Redox Flow Batteries

Miguel Cantera,[a] Koray Cavusoglu,[c] Lara Lubián,[b, c] Rubén Rubio-Presa,[c] Roberto Sanz,[c] Virginia Ruiz,[b, c] Jose María Cámara,*[a] and Edgar Ventosa*[b, c]

Aqueous Organic Redox Flow Batteries (AORFBs) have received much attention due to the accessibility of their active materials. However, among the key performance indicators that require improvement for AORFBs to become competitive against mature technologies, lifespan is especially critical for stationary energy storage. Faradaic imbalance driven by the occurrence of irreversible electrochemical processes decreases lifespan, so monitoring and correction of this parameter is required to prolong lifespan. This work presents a novel, simple and non-invasive automatized method to monitor the Faradaic imbalance. This method is based on detecting the variation of the minimum derivative of the cell voltage upon cycling, and it is used as the activation criterion for a rebalancing device. The system is tested using an alkaline flow battery consisting of ferrocyanide and 2,6-dihydroxyanthraquinone (2,6-DHAQ), extending the cycle life of the battery to 400 cycles (235 h) without any capacity decay and without Ar-filled glovebox. This demonstrates the feasibility of the proposed system to monitor the state-of-health (SOH) due to Faradaic imbalance and recover the capacity loss.

1. Introduction

The use of fossil fuels is the main source of human greenhouse gas emissions, which are responsible for Earth's global warming.[1] Renewable energy sources are a promising alternative to reduce the emissions significantly in the long-term.[2] However, their intermittent nature requires the implementation of energy storage systems (ESS) to level supply-demand in the grid at any moment. There are several types of ESS, being classified into electrochemical, mechanical, electrical and thermal.[3] Pumped hydro storage is by far the most popular, with an installed power capacity of 172.5 GW, which accounted for 90% of the total share in 2020.[4] However, this technology has geographical constraints[5] and presents a notable impact on nature conservation.[6] On the other hand, electrochemical ESS offer advantages such as flexibility or short construction cycle time.[7] While Li-ion batteries largely dominate sectors such as electric vehicles or consumer electronics, its use for stationary energy storage is limited by safety and scalability restrains, among others.[8] Redox flow batteries (RFBs), that are featured by their flexible and scalable configuration due to its independency between power and energy,[9] represent a promising EES. The All-Vanadium Redox Flow Battery (VRFB), that was initially proposed in the 1980s and refined during the last decades, is considered the most pursued and researched RFB,[10,11] reaching a total energy capacity installed globally of around 1.5 GWh.[12] Unfortunately, the supply chain for VRFB raises concerns since Vanadium is considered a critical material.[13,14] Consequently, other alternatives have been explored. RFBs based on more abundant inorganic materials, such as Zn–Fe RFB, are a promising alternative.[15] Aqueous Organic Flow Batteries (AORFBs) that employ redox-active organic compounds dissolved in the electrolytes have also attracted much interest in the last 15 years.[16] Organic compounds not only are based on carbon, but they offer the distinct advantages of improving key performance indicators by fine-tuning their structure through molecular engineering, providing a high degree of flexibility in terms of solubility, electron transfer, crossover reduction, chemical and electrochemical stability and reaction kinetics.[17] Several chemistries have shown promising performances, including viologen derivatives – TEMPO-derivatives in neutral pH and anthraquinone derivative – ferrocyanide in alkaline media.[18–21] While these systems have achieved remarkable performance, AORFB technology still needs to overcome certain limitations to become competitive against more matured RFBs like All-Vanadium.

Commercial success and market penetration of RFBs requires enhancing lifespan and reducing costs.[22] State-of-health (SOH) monitoring is essential for the former aspect, so that corrective actions are timely taken.[23,24] SOH reflects the deviation of the battery's current condition from its initial design specifications, typically calculated as the ratio of current energy storage capacity to its maximum capacity. Factors

[a] M. Cantera, J. María Cámara
Department of Electromechanical Engineering, University of Burgos, Avenida Cantabria s/n. E-09006 Burgos, Spain
E-mail: checam@ubu.es

[b] L. Lubián, V. Ruiz, E. Ventosa
International Research Centre in Critical Raw Materials-ICCRAM, University of Burgos, Plaza Misael Bañuelos s/n, E-09001 Burgos, Spain
E-mail: eventosa@ubu.es

[c] K. Cavusoglu, L. Lubián, R. Rubio-Presa, R. Sanz, V. Ruiz, E. Ventosa
Department of Chemistry, University of Burgos, Plaza Misael Bañuelos s/n, E-09001 Burgos, Spain

Supporting information for this article is available on the WWW under https://doi.org/10.1002/batt.202400737

Research Article
doi.org/10.1002/batt.202400737

contributing to SOH reduction include electrolyte degradation, crossover of species through the membrane, and Faradaic imbalance between anolyte and catholyte.[25–28] Electrolyte degradation has been intensively investigated,[29,30,18] showing that great improvements can be achieved through molecular engineering. Crossover can be mitigated by molecular engineering (larger active species) and polymer science (adjusting the properties of the ion-selective membrane). There are examples showing that crossover can be prevented.[31–33] The Faradaic imbalance has been generally overlooked in AORFBs although there are few studies in the literature.[34,35,23]

Methods used for state-of-charge (SOC) estimation can be employed to estimate SOH, as both metrics are closely related to the amount of stored charge. While measuring open-circuit voltage (OCV) is a common approach,[36] combination of OCV with equivalent circuit models (ECMs) can provide real-time accuracy estimation.[37] However, their accuracy is often limited, particularly for long-term operations and slow capacity loss. Attempt to reduce the complexity considering 0D VRFB models, compared to 1D and 2D models, resulted in improved results, but SOH estimation accuracy was still constrained.[38] Two main improvements have been proposed to address these limitations. On the one hand, hybrid methods combine models with physical measurements. For instance, Vlasov et al. proposed the combination of OCV measurement with the refractive index value measured by an optical fiber in the anolyte.[39] Other approaches developed methods characterized by using a limited number of sensors (voltage and current measurements) to estimate SOH with around 2% error.[40] On the other hand, custom-designed monitoring sensors have been implemented in RFBs. For instance, Schubert et al. developed a system based on Arduino that estimates SOC, SOH, and electrolyte capacity using Coulomb counting.[41] Finally, other invasive sensors can measure both relative species concentration and magnitude, enabling simultaneous monitoring of SOC and SOH.[42] In summary, each of the methods proposed in the literature possesses advantages but also entails constraints. In any case, intense research activity in this area illustrate that the development of accurate, non-invasive, and cost-effective methods remains a crucial challenge for bringing RFBs closer to the market.

In this context, this work presents a novel, non-invasive method suitable for industrial applications to monitor state-of-health (SOH) degradation resulting from Faradaic imbalance in AORFBs. A low-cost battery management system (BMS) is used to implement and validate the proposed method. The underpinning fundaments of the method are first discussed to establish its feasibility for SOH monitoring. Galvanostatic measurements are conducted to validate the initial hypothesis with empirical data. Subsequently, the method is integrated into the BMS without a rebalancing device to assess its ability to detect SOH variations. An electrochemical rebalancing system that is able to effectively reverse the effects of the Faradaic imbalance is added to the BMS to recover capacity. The new method is used as input to determine when the rebalancing system needs to be activated. To monitor the SOH using an independent method, discharge capacity is simultaneously recorded by counting the charge stored in full cycles using a battery testing system, which on the other hand is not practical in industrial scenarios. The results obtained in a full battery demonstrate that the battery can operate for extended periods without significant capacity loss. This advancement paves the way for AORFBs to become more competitive technologies for stationary energy storage.

Experimental Section

Chemicals

All common reagents and solvents were purchased from Aldrich or Alfa-Aesar and used as received without further purification. The resin used for 3D printing of the rebalancing cell was a UV transparent resin (Anycubic).

Redox Flow Battery

This study uses a battery reactor formed by a two filter-pressed flow semi-cells using Nafion NRE-212 (Ion Power, USA) as the ion selective membrane, graphite felt (SIGRACELL GFD 2,5 EA, SGL Carbon) as the electrode and expanded graphite (bipolar plate SIGRACELL TF6, SGL Carbon) as the current collector. Viton® gaskets of 2 mm and 1 mm thickness were used for the batteries and the rebalancing cell respectively due to its resistance to alkaline conditions. The projected area of the cell was 10 cm^2. A MasterFlex L/S peristaltic pump was used to provide a flow rate of 35 $mL\,min^{-1}$. While the composition of the electrolytes was always the same, the volumes were slightly changed, as indicated in the corresponding figure captions. In particular, two conditions were used: I) 11.3 mL of 0.3 M potassium ferrocyanide in 1 M KOH for the catholyte and 10 mL of 0.2 M of 2,6-DHAQ in 1 M KOH for the anolyte. II) 13 mL of 0.3 M potassium ferrocyanide in 1 M KOH for the catholyte and 11.7 mL of 0.2 M of 2,6-DHAQ in 1 M KOH for the anolyte. Detailed information about the synthesis of 2,6-DHAQ is provided in the Supporting Information, section S2.

Electrochemical Characterization

Charge-discharge cycles on the battery were conducted using a Neware BTS4000. The current density used was $\pm 30\,mA\,cm^{-2}$ with voltage limits of $+1.6$ V for charge and $+0.5$ V for discharge.

Data Acquisition and Rebalancing System

For the cell voltage measurement, an ADC ADS1115 breakout board from Adafruit was connected to an MDUINO 38 R PLC using I^2C communication protocol. Galvanic isolation is implemented using an Adum1250 digital isolator. The data is sent from the MDUINO to a Raspberry Pi 4 using a 5 V TTL to USB serial converter. A rebalancing membrane-free flow device placed in the catholyte tank was used. Dimensions of the expanded graphite were 3×2 cm. The platinum filament length was 1.5 cm, the diameter was 0.5 mm and had a 99.95% purity. The rebalancing device was controlled by one of output relays of the MDUINO, which applied a dedicated 1.2 V fixed voltage to the device when closed.

Research Article
doi.org/10.1002/batt.202400737
Chemistry Europe
European Chemical Societies Publishing

2. Results and Discussion

2.1. Fundaments of the Method

The new method proposed in this work focuses on the estimation of the Faradaic imbalance between the anolyte and catholyte, which is a primary source of SOH degradation arising from Faradaic imbalance. This imbalance is originated from the occurrence of irreversible parasitic reactions. For the chemistry studied in this work, oxygen reduction reaction (ORR) and hydrogen evolution reaction (HER) occurring in the anolyte are the specific irreversible parasitic reactions occurring.[35] These reactions irreversibly consume charge during the charging step, leading to accumulation of oxidized (charged) active species in the catholyte. Consequently, the amount of charged species in the catholyte and anolyte are different at the end of charging step, which is so called Faradaic imbalance. This mismatch in the SOC of both electrolytes limits the discharge step since the process is stopped by the anolyte, resulting in incomplete catholyte discharge. While the Faradaic imbalance may be slow, its gradual and irreversible nature accumulates over time, degrading the SOH in the long term. Detection of the Faradaic imbalance should in principle require measuring the SOC of both electrolytes separately. At this point, it is important to note that measuring OCV provides information about the overall SOC, not the individual electrolyte SOCs. The term OCV is derived from the following expression (Equation (1)):

$$OCV = E_c - E_a \tag{1}$$

Where E_c and E_a are the redox potential of the catholyte and anolyte, respectively. In turn, both redox potentials are determined by the Nernst equation (Equation (2)):

$$E = E_0 + \frac{RT}{zF} \ln\left(\frac{a_{ox}}{a_{red}}\right) \tag{2}$$

The relationship between redox potential and SOC is expected to be symmetrical for both anolyte and catholyte. Due to Equation (2), the redox potential changes rapidly at low and high SOC levels, approaching a plateau near 50% SOC. Figure 1A illustrates this theoretical evolution of redox potentials with SOC. The differential plot of redox potential over SOC in Figure 1C shows steep slopes at both low and high SOC, with a minimum (or maximum) at 50% SOC. Figure 1B shows the OCV, which is the difference between the catholyte redox

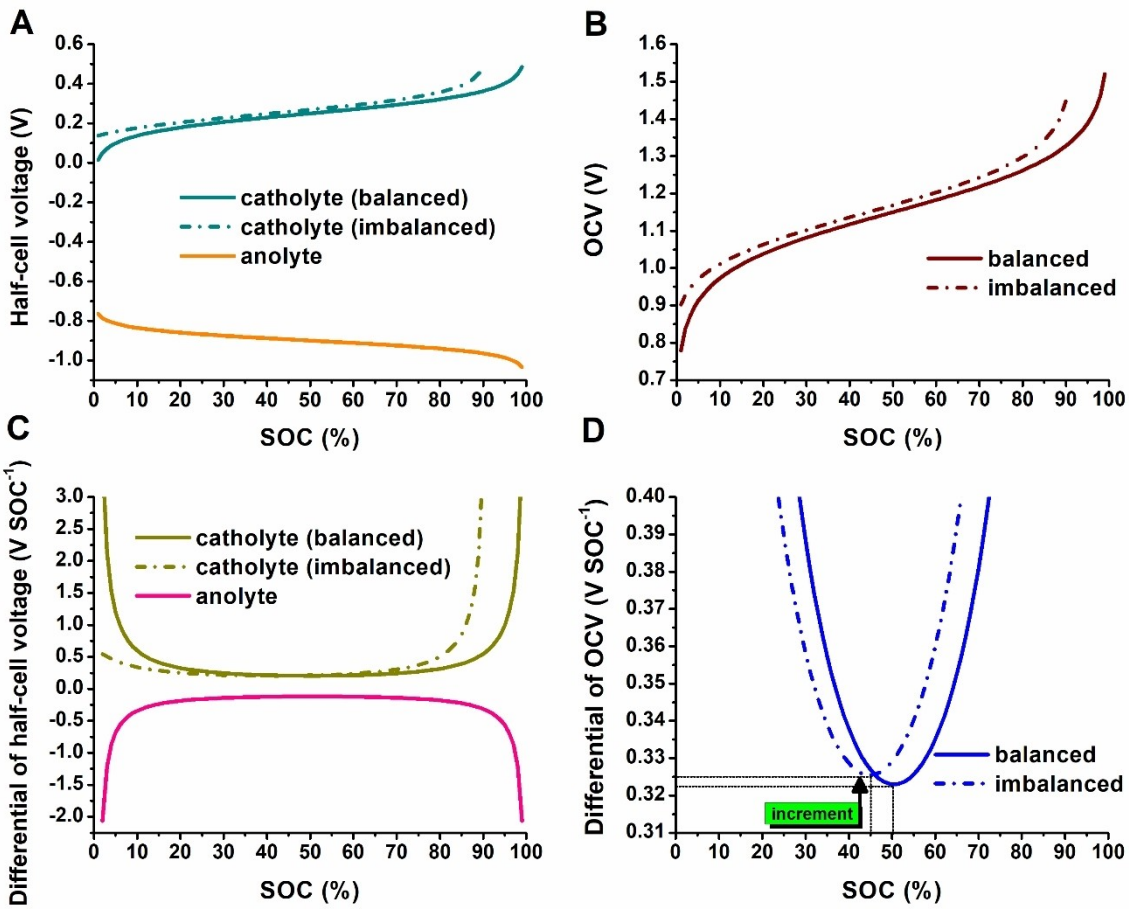

Figure 1. (A) Theoretical (simulated) evolution of the half-cell redox potentials for catholyte and anolyte for both balanced and imbalanced cycles (B) Evolution of the cell voltage for both balanced and imbalanced cycles (C) Evolution of the differential of the half-cell redox potentials for the catholyte and anolyte for both balanced and imbalanced cycles (D) Zoom of the evolution of the differential of the OCV for both balanced and imbalanced cycles.

Research Article
doi.org/10.1002/batt.202400737
Chemistry Europe
European Chemical Societies Publishing

potential (E_c) and the anolyte redox potential (E_a). Therefore, its behavior is influenced by the individual redox potentials. In a balanced battery, the differential plots for E_a and E_c should be synchronized, reaching 50% SOC simultaneously. However, Faradaic imbalance leads to misalignment of these curves, resulting in a mixed behavior for the V_{cell} differential plot. Notably, a mismatch in the minima or maxima of E_a and E_c will cause a broader minimum with a higher absolute value in the OCV differential plot, as shown in Figure 1D. This characteristic suggests that the value of the minimum in the OCV differential plot could potentially be used to estimate the Faradaic imbalance in the system. It is important to note that the data in Figure 1 is theoretical and not based on actual measurements. In this hypothetical case, the minimum derivative of the OCV over SOC changes from 0.3230–0.3254 when the cell becomes imbalanced due to SOC desynchronization between anolyte and catholyte.

2.2. Experimental Validation

Since the Battery Test System (BTS) cannot calculate by itself the derivative of the cell voltage (V_{cell}), a Python program was developed to approximate this value using finite differences. Given the discrete nature of V_{cell} measurements, a backward finite difference approximation was employed:

$$f'(x_i) \approx \frac{y_i - y_{i-1}}{x_i - x_{i-1}} \tag{3}$$

Where $y_i$is the V_{cell} value; y_{i-1} is the previous V_{cell} value; x_i is the time stamp in seconds of the current V_{cell} value; x_{i-1} is the time stamp in seconds of the previous V_{cell} value. The BTS registers V_{cell} readings every second. However, due to the low accuracy of V_{cell} measurement coming from the BTS, the derivative of V_{cell} over capacity was calculated every 10 samples (20 seconds) instead of every second. This allows to smoothen the differential curve. In addition, a simple normal averaging of the last 10 derivative samples was applied. Further details about normal averaging are provided in Supporting Information Section S7. Figure 2 illustrates the V_{cell} and its differential plot for a balanced cycle (cycle 1, 100% capacity retention) and for an imbalanced one (cycle 30, 89% capacity retention). The differential plot values exhibited a bath-shaped curve for both cycles, having the minimum value at approximately 50% SOC. In cycle 30 (imbalanced), the value of the minimum for the differential curve was higher (0.1365 mV mAh^{-1}) than that of cycle 1 (balanced, 0.1305 mV mAh^{-1}). The differences between the value of the minimum are 10 times larger than the noise (0.0115 mV mAh^{-1}) of the differential curve (corrugated signal around the minimum), so that further smoothing is not required. Therefore, these results confirm the hypothesis that

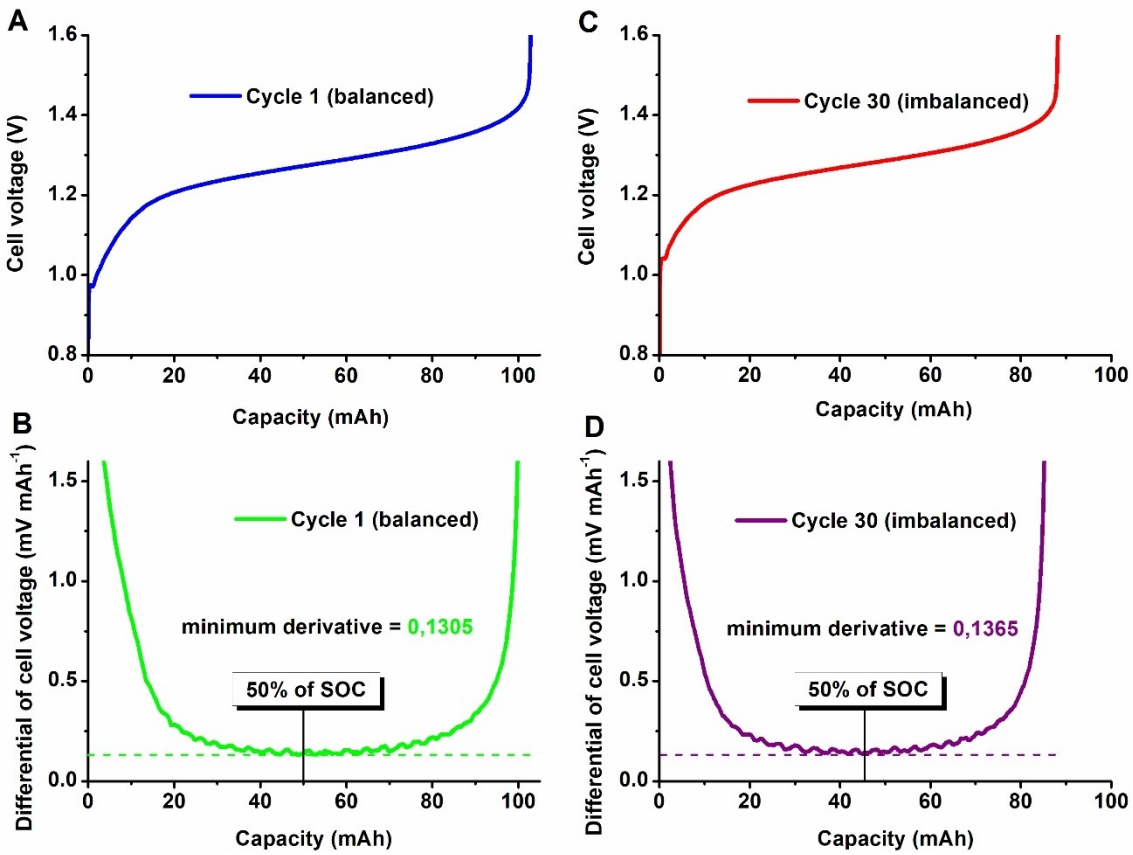

Figure 2. (A) Evolution of the cell voltage and (B) its differential plot during the charging process with respect to its capacity when the battery is balanced (C) Evolution of the cell voltage and (D) its differential plot during the charging process with respect to its capacity when the battery is imbalanced.

increasing level of imbalance leads to an increase in the minimum derivative value. This suggests that a PLC can effectively detect the Faradaic imbalance by monitoring the evolution of the minimum derivative value. While the method has been validated for the charging step, it can also be applied to discharging steps by taking the absolute value of the derivative.

2.3. Automatization of the Method

The minimum derivative value method proposed in this work is implemented on the same BMS used in our previous work,[35] where a PLC is used to create an automatic control loop. Although the main input of the system is still the instantaneous V_{cell}, the software PLC program code is updated to calculate its derivative. This value is then used as the criterion for the activation of the rebalancing device. Figure 3 shows the simplified design diagram of the automatized rebalancing system.

Simultaneously, a BTS is used to register the evolution of the discharge capacity during the cycling process. These values from the BTS will be employed to verify the new method since the SOH can be directly determined from the charge storage capacity (full cycles). While the basis of the rebalancing system was adopted from our previous work, some modifications were necessary to implement this new SOH estimation. For instance, it was required to replace the PC by a Raspberry Pi to receive the data from the PLC in a more stable way. The use of Raspberry Pi not only reduces the cost and size but also increases the reliability and stability of the system (check Supporting Information, Section S4 for complete details). Besides, the smaller connectors used for the V_{cell} measurements as well as for the connectors used between the rebalancing device and the fixed power supply voltage were used to facilitate proper connections. At software level, several changes were implemented to accomplish two objectives: I) improve the accuracy of the V_{cell} measurement; II) calculate its derivative in real-time. I) The former is of crucial important as the most accurate reading possible is needed to detect the change in the derivative. Meanwhile, V_{cell} value coming from the ADC was loaded into a float data-type variable. As an interruption could come at any moment in time, it also could occur that an interrupt happens when the main code has halfway updated the float variable, which is wider than 8-bit. When this kind of event happened, the value of V_{cell} was not updated (using one similar to the latest one). As a result, both V_{cell} and its derivative values were distorted, making harder to detect variations in the derivative. The interrupts were addressed using Arduino *millis()* function, which returns the time in milliseconds passed since the beginning of the execution of the program. Additionally, to align the data-type used, the ADC raw value reading is stored in an int data-type and then stored into a float, as it needs to be scaled. II) The latter change in the code was introduced to enable real-time estimation of the derivative of the V_{cell}, using Equation (3). Due to the high accuracy of V_{cell} measurement obtained from the external ADC, the derivative is calculated in the PLC every sample (2 seconds). To smoothen even more the resulting derivative signal, two normal averaging are performed. Firstly, before the V_{cell} value is printed into the text file, a normal averaging of the last 7 V_{cell} samples is applied. Secondly, another similar 7 sample normal averaging is done to the derivative signal obtained from V_{cell}. The reason for using 7 samples for each averaging was because it was considered enough time to finally obtain a sufficiently smooth signal to detect the minimum derivative variations per cycle. Both

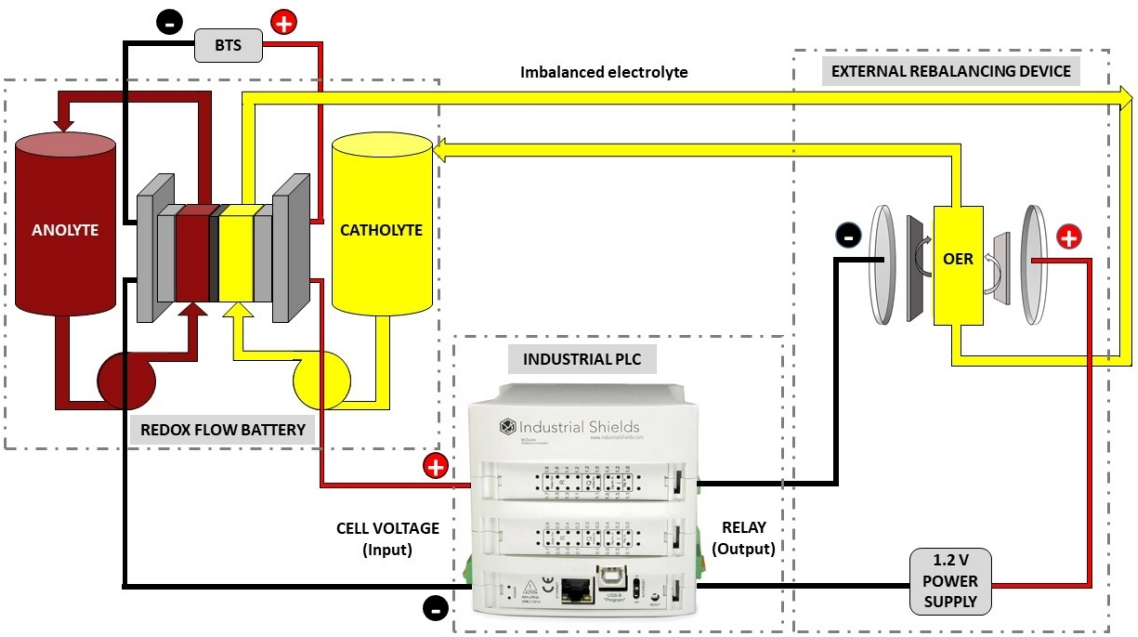

Figure 3. Simplified diagram design of a RFB with the proposed rebalancing device controlled by a PLC. The cell voltage is measured by the PLC from the battery reactor. Then the PLC computes the cell voltage derivative, which is used as the criterion to control the rebalancing device.

operations imply a total delay for the rebalancing device criterion activation of 28 seconds. As normally each charging/discharging cycle last minutes and the minimum derivative value is located in the middle of each cycle, this delay is acceptable to activate/deactivate the rebalancing device during each cycle. Although *millis()* function has an accuracy around ± 50 milliseconds, this does not affect the measurement as the value is too small compared with the delay of the average filter implemented.

The criterion for the activation of the rebalancing device needs to be established. To this end, the PLC will store the minimum derivative value of each charging cycle $D_m\ (current)$. Besides, the PLC will store one of these cycles as the historic minimum derivative. This will be considered as the reference one and will be denominated $D_m(reference)$. This $D_m(reference)$ value can be configured to be the first cycle (default configuration), but it can also be set to be a value specified by the operator manually in the PLC program code. It will be considered that the battery is in imbalance state if the following criterion is fulfilled:

$$Imbalance \leftrightarrow \frac{D_m\ (current) - D_m\ (reference)}{D_m\ (reference)} \times 100 > q \qquad (4)$$

q is a percentage that can also be configured in the code and is set in the experiment by default to 10%. This means that if the difference between $D_m\ (current)$ and $D_m\ (reference)$ divided by $D_m\ (reference)$ in percentage is higher than the configured limit, then the battery is considered to be in an imbalanced state and the rebalancing device shall be activated. As this criterion is implemented using the charge cycles, the $D_m\ (current) >= D_m\ (reference)$ as the D_m always increases along cycling. Thus, the difference between of $D_m\ (current) - D_m\ (reference)$ is always positive. However, if discharge cycles are used, the difference shall be taken in absolute value, because D_m always decreases along cycling. Finally, the PLC will perform the rebalancing process by controlling the opening/closing (OFF/ON) of one of its digital output relays. This will allow the rebalancing device to be biased by a 1.2 V power supply enabling the rebalancing process to take place. The complete PLC program source code and the configuration values are included in the Supporting Information section S5.

2.4. Implementation in Anthraquinone – Ferrocyanide Flow Battery in Alkaline Media

An alkaline anthraquinone – ferrocyanide (An–Fe) redox flow battery was selected to evaluate the proposed method (a photograph of the full system is displayed in Supporting Information Figure S1). In this system, the imbalance between the SOC for catholyte and anolyte is driven by the irreversible process occurring in the anolyte, i.e., oxygen reduction reaction and hydrogen evolution (Figure 4A). For the sake of the explanation, let assume that hydrogen evolution takes place in the anolyte. In that case, anolyte will not be able to reach a fully charged state, while the catholyte will. In the discharge, the anolyte will be the limiting side since it was not fully charged. As a result, the discharge capacity will shorten, and the catholyte will not be fully discharged. In the subsequent cycle, the catholyte will start partly charged, which will reduce the capacity for the second cycle. In fact, the accumulation of charged catholyte at the end of the discharge step leads to irreversible and accumulative loss in capacity. This process is referred to as Faradaic imbalance. Promoting the occurrence of an irreversible process in the catholyte, i.e., the oxygen evolution reaction (OER), leads to the rebalancing of the SOC for catholyte and anolyte (Figure 4B). In other words, promoting the opposite reaction in the opposite side leads to cancelling effect. A simple way of promoting OER is to lift the upper cut-off voltage from 1.6 V–2.0 V.[34] While this approach is simple, its long-term implementation can lead to corrosion issues in the carbon-based electrodes. Additionally, this strategy requires

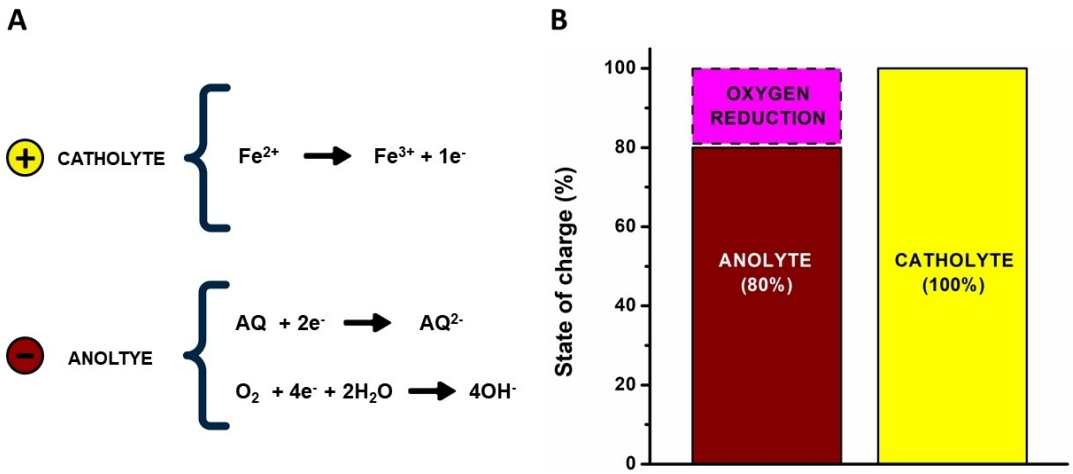

Figure 4. Scheme illustrating the processes involved in the Faradaic imbalance of an An–Fe redox flow battery (A) Reactions involved during the charging process, where the anolyte suffers from both reversible and irreversible reactions (B) Imbalance in the state of charge between anolyte and catholyte at the end of the charging process.

Research Article
doi.org/10.1002/batt.202400737
Chemistry Europe
European Chemical Societies Publishing

deep charge. Thus, decoupling of the OER outside the electrochemical reactor was proposed as a more practical approach. An effective rebalancing system that promotes the OER to reverse the Faradaic imbalance was recently demonstrated.[35] Monitoring of the Faradaic imbalance to control the rebalancing system remains a challenge.

In this context, our method to monitor the Faradaic imbalance was initially assessed using the first simple approach where the imbalance was corrected by changing the upper cut-off voltage. The monitoring method was implemented by estimating the minimum value of the derivative per charging cycle, while the charge stored measured by the BTS was used to determine the level of Faradaic imbalance. Figure 5A shows the evolution of the discharge capacity registered by the BTS. The capacity continuously decreased until the charging protocol is changed in cycle 110. It should be noted that the slight change in the slope of the capacity fading is unknown, while it is expected that a change in the Ar pressure affects the entry rate of air in the anolyte. The evolution of the derivative of the V_{cell} for each cycle (computed by the PLC) is plotted in Figure 5B. It can be checked that as the capacity decreases, the minimum derivative value increases proportionally. This initial measurement intended to assess whether the BMS has enough sensitivity to detect the minimum derivative variation along the cycling and verify whether this parameter is a feasible criterion for the activation of the rebalancing device. The initial 7 cycles were carried out using 2.0 V as upper cut-off voltage, instead of 1.6 V. By doing this, the oxygen evolution reaction in the catholyte is enabled compensating the charges consumed irreversibly in the anolyte. This means that the charge stored measured by the BTS remained stable for these first 7 cycles. After that, the upper cut-off voltage was lowered to 1.6 V (standard cycling conditions). Under these conditions, the OER in the catholyte is not allowed, so that slow oxygen entering leads to irreversible process occurring in the anolyte, resulting in progressive Faradaic imbalance (and the corresponding capacity fading). This process can be checked also in Figure 5C, where the evolution of the V_{cell} is shown for four different cycles: balanced cycles (1 and 115) and imbalanced cycles (100 and 110). As a result of the Faradaic imbalance, the charge stored measured by the BTS gradually decreased during the following 100 cycles. After 110 cycles, the upper cut-off voltage is lifted to 2.0 V, so that the OER in the positive electrode is allowed during the last 10 cycles. The voltage profile for cycle 110 shows the occurrence of a second plateau, which corresponds to the OER in the positive electrode and the reduction of anthraquinone in the negative electrode. Once all anthraquinone is reduced, the plateau ends. The potential in the negative electrode would evolve till HER occurs, but the occurrence of OER and HER at these conditions requires more than 2.0 V, so that charge stops before this happens. The charge stored measured by the BTS immediately recovered its initial value. The evolution of the minimum derivative value followed the trend of the charge stored measured by the BTS: as the stored capacity decreased, the minimum derivative value increased. Remarkably, the minimum derivative value recovered its initial values for the last 10 cycles, when the upper cut-off voltage is lifted to 2.0 V and the stored capacity returned to its

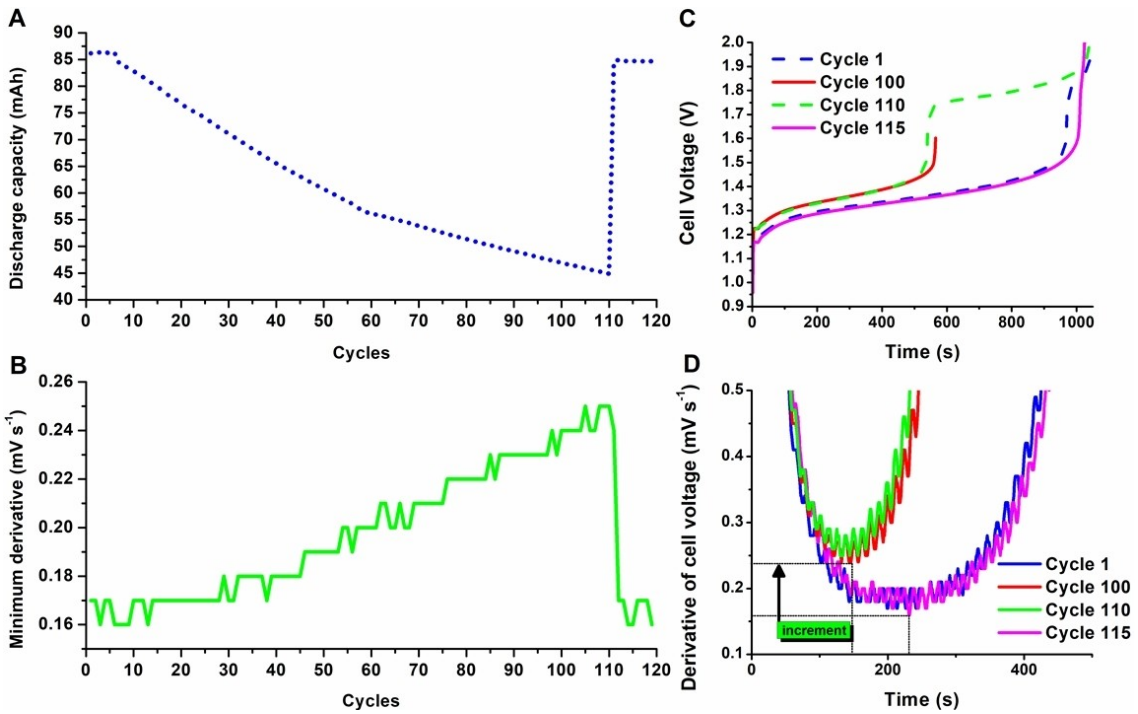

Figure 5. Evolution of the (A) discharge capacity and (B) the minimum derivative during 120 cycles using the BTS manually as the rebalancing system (C) Evolution of the cell voltage measured by the BTS sampled every second (D) Evolution of the derivative of the cell voltage over time computed by the PLC every 2 seconds. Catholyte: 11.3 mL of 0.3 M potassium ferrocyanide in 1 M KOH; anolyte: 10 mL of 0.2 M of 2,6-DHAQ in 1 M KOH. Cut-off voltage for charging cycles is 1.6 V except during the rebalancing operation, when it is set to 2.0 V.

original value. Specifically, as it is shown in Figure 5D and due to the progressive entrance of oxygen in the system, the minimum derivative per charging cycle increases from 0.16–0.17 $mV s^{-1}$ (cycle 1) to a maximum of 0.25 $mV s^{-1}$ (cycle 100). After the application of the electrochemical rebalancing using the BTS, the minimum derivative decreased again to 0.16–0.17 $mV s^{-1}$ (cycle 115).

After validating the method for monitoring the Faradaic imbalance, it was integrated into our BMS. Specifically, the PLC records the evolution of the cell voltage, computes its derivative and automatically activates the rebalancing device based on this analysis. From now on, only the minimum derivative per cycle is registered by the PLC, in order to reduce the amount of data stored into the data file. As first criterium, $q = 10\%$ from Equation (4) was selected to activate the rebalancing device. That is, when the difference between the reference value of the derivative and the value obtained for a given cycle is above 10%, the battery will be assumed to be imbalanced and the rebalancing device will be activated. For more details about other software updates, check Supporting Information, Section S6. Figure 6A shows the evolution of the discharge capacity in a fully automatized measurement and Figure 6B shows the evolution of the minimum derivative. At the first cycle, the PLC computes a $D_m = 0.1518\ mV s^{-1}$, which is stored as $D_m(reference)$. As $q = 10\%$ was selected, using Equation (4), the minimum derivative shall reach a value of at least 0.1669 so that the rebalancing device can be activated. Since the battery is slightly limited by the capacity of the catholyte (104.5 mAh and 109.7 mAh for catholyte and anolyte respectively), the Faradaic imbalance due to the occurrence of irreversible process in the anolyte leads to an immediate capacity fading. After 56 cycles, the value of the minimum of the derivative was 0.1684 which is larger than $D_m(reference)$. Consequently, the rebalancing device was activated in that cycle for the first time. In fact, the rebalancing device was activated for the 5 subsequent cycles. As a result, the capacity fading ceased. The rebalancing device was intermittently activated for the subsequent cycles (indicated in Figure 6A), leading to a stabilization of the discharge capacity at ca. 83 mAh. Consequently, the discharge capacity was stabilized at 86.5% of the initial value.

While it was shown that the method can be used to monitor the level of Faradaic imbalance, the set criterium of $q = 10\%$ in the value of the minimum of the derivative curve left room for improvement. However, selecting a value excessively small brings the risk of over-balancing. That is, the charges consumed by the OER taking place in the rebalancing device exceeds that of the irreversible process in the anolyte. In that case, the PLC would understand that the system is imbalanced and would activate the rebalancing device, which would worsen it. To address this risk, a smaller Pt wire was used in the rebalancing device for the next experiment (0.5 cm vs 1.5 cm, 0.5 mm diameter in both cases). Additionally, the value of q was reduced from 10% to 5%. As a result, the rebalancing device should be activated more times to reverse the Faradaic imbalance. Figure 7A and Figure 7B show the evolution of the discharge capacity upon cycling together with the frequency activation of the rebalancing device. In this experiment, the PLC computes a $D_m(reference) = 0.1492\ mV s^{-1}$. As $q = 5\%$ was selected, using Equation (4), the minimum derivative shall reach a value of at least 0.1566 in order to activate the rebalancing device. The presence of oxygen in the anolyte drives the Faradaic imbalance over the first 100 cycles leading to a gradual decrease in capacity. In the cycle 13, the PLC autonomously activated the rebalancing device and kept activating it for 250 cycles. As a result, not only the capacity fading was ceased, but the initial capacity was almost recovered (96% of the initial capacity). After that point, the rebalancing device was activated few tens of times to maintain the capacity stable. It is hypothesized that the oxygen level in the system was probably higher at the beginning of the measurement, e.g., small amount of oxygen that is difficult to be purged without the use of an Ar-filled glovebox. After that, the oxygen entering rate is relatively low, which does not require the activation of the rebalancing device with high frequency. Figure 7C shows the evolution of the minimum derivative along the cycling. Due to

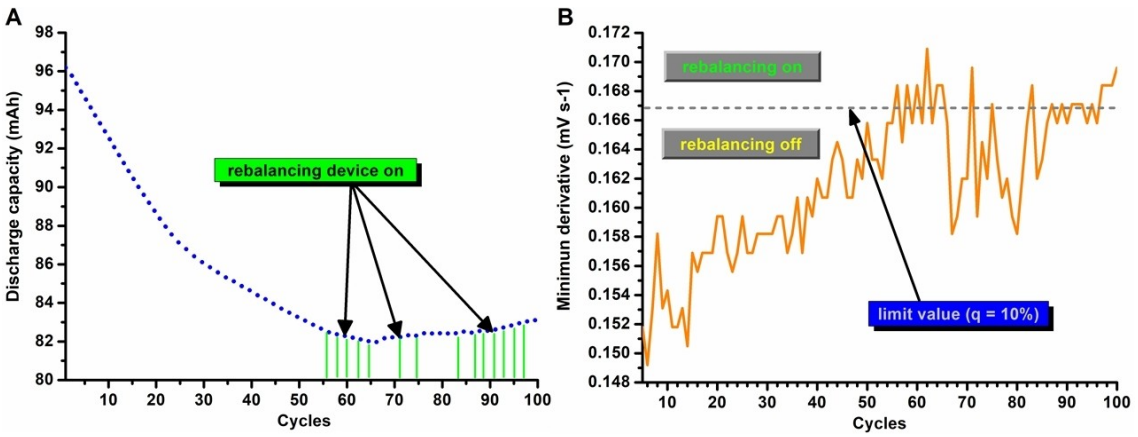

Figure 6. (A) Evolution of the discharge capacity using the automatic rebalancing device system with $q = 10\%$. Vertical green lines mark when the PLC applies the fixed voltage to activate the rebalancing device, which was done a total of 15 times (B) Minimum derivative evolution along charging cycles during the experiment with q = 10%. The limit value dictates when the rebalancing device is activated (above the limit) or deactivated (below the limit). Catholyte: 13 mL of 0.3 M potassium ferrocyanide in 1 M KOH; anolyte: 11.7 mL of 0.2 M of 2,6-DHAQ in 1 M KOH. Cut-off voltage for charging cycles is 1.6 V.

Research Article
doi.org/10.1002/batt.202400737
Chemistry Europe
European Chemical Societies Publishing

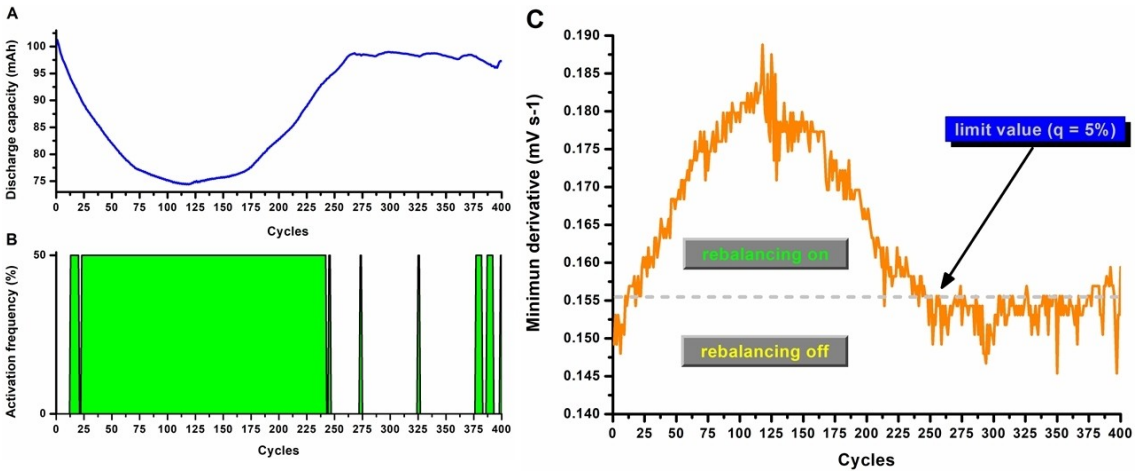

Figure 7. (A) Evolution of the discharge capacity and (B) the frequency of the rebalancing device activation during the experiment with $q = 5\,\%$. (C) Minimum derivative evolution along charging cycles for the same experiment. The limit value dictates when the rebalancing device is activated (above the limit) or deactivated (below the limit). Catholyte: 13 mL of 0.3 M potassium ferrocyanide in 1 M KOH; anolyte: 11.7 mL of 0.2 M of 2,6-DHAQ in 1 M KOH. Cut-off voltage for charging cycles is 1.6 V.

an increase in the ambient temperature in the end of spring, the Raspberry overheated and stopped working. This terminated the measurement after 400 cycles and almost 10 days (235 hours), which on the other hand is a sufficiently long period to demonstrate the feasibility of the method. A heat sink with an active fan should be used permanently to avoid this issue. It should be noted that the use of non-commercial organic materials (e.g., 2,6 dihydroxy anthraquinone) leads to minimization of the full battery system, so that low amounts of active materials are required. This fact results in application of current densities that enable that charge and discharge steps last for at least 30 min. In other words, despite alkaline AORFB can operate at higher current densities (e.g., 80 mA cm^{-2}), the standard conditions at lab scale and thus scientific articles are in the range of 20–40 mA cm^{-2}. The fundaments of our proposed method are not influenced by the current densities since the derivative represent the variation of cell voltage with the SOH.

3. Conclusions

SOH monitoring is one of the most important functionalities of a BMS to provide a robust operation of an RFB and assure its performance. With this context, this work proposed a new simple and non-invasive method that was capable of monitoring the SOH related to the Faradaic Imbalance through evaluation of the minimum value of the derivative curves of the cell voltage over SOC. A PLC was used to register the cell voltage, compute its derivative in real-time and register the minimum derivative value of each charging cycle. The first cycle was used as a reference, which was compared against the minimum derivative of the current cycle. When the minimum derivative relative difference between the current cycle and the reference cycle was larger than a fixed limit value, the battery was considered to be in imbalanced state. This criterion was used by the PLC to activate the rebalancing device so the capacity loss can be recovered. An experimental validation was done against the evolution of the capacity measured by the BTS, where the battery was able to reach 400 cycles keeping the capacity at around 96 % of its initial value. In contrast, without this BMS, it would not have surpassed even 50 cycles due to Faradaic Imbalance. In contrast to already existing methods, this study presented a simple and non-invasive approach suitable for commercial applications that monitors the SOH of the redox flow battery and is used by our BMS as a criterion to recover the capacity loss. This allows the extension of the battery lifetime to its maximum practical value, paving the way to more competitive AORFBs.

Acknowledgements

The authors acknowledge financial support by the Spanish Government (Ministerio de Ciencia e Innovacion, Grants PID2021-124974OB-C22, CNS2023-145051, PID2023-148198NB-C21) and Ramon y Cajal award (RYC2018-026086-I) as well as the MeBattery project. MeBattery has received funding from the European Innovation Council of the European Union under Grant Agreement no. 101046742. This work was supported by the Regional Government of Castilla y Leon (Junta de Castilla y Leon), the Ministry of Science and Innovation MICIN and the European Union NextGenerationEU/PRTR (C17. I1).

Conflict of Interests

The authors declare no conflict of interest.

Research Article
doi.org/10.1002/batt.202400737

Data Availability Statement

The data that support the findings of this study are available on request from the corresponding author. The data are not publicly available due to privacy or ethical restrictions.

Keywords: Fadaday imbalance · aqueous organic redox flow batteries · state of health · rebalancing · cell voltage

[1] J. E. Hansen, M. Sato, L. Simons, L. S. Nazarenko, I. Sangha, P. Kharecha, J. C. Zachos, K. von Schuckmann, N. G. Loeb, M. B. Osman, Q. Jin, G. Tselioudis, E. Jeong, A. Lacis, R. Ruedy, G. Russell, J. Cao, J. Li, *Oxford Open Climate Change* **2023**, *3*, kgad008.
[2] L. Al-Ghussain, *Environ. Prog. Sustain. Energy* **2019**, *38*, 13.
[3] O. Palizban, K. Kauhaniemi, *J. Energy Storage* **2016**, *6*, 248.
[4] M. Y. Worku, *Sustainability (Switz.)* **2022**, *14*, 5985.
[5] P. Das, B. K. Das, N. N. Mustafi, M. T. Sakir, *Energy Storage* **2021**, *3*, e223.
[6] B. Steffen, *Energy Policy* **2012**, *45*, 420.
[7] T. Chen, Y. Jin, H. Lv, A. Yang, M. Liu, B. Chen, Y. Xie, Q. Chen, *Trans. Tianjin Univ.* **2020**, *26*, 208.
[8] D. Reber, S. R. Jarvis, M. P. Marshak, *Energy Adv.* **2023**, *2*, 1227.
[9] J. Girschik, L. Kopietz, M. Joemann, A. Grevé, C. Doetsch, *Chem. Ing. Tech.* **2021**, *93*, 523.
[10] K. Lourenssen, J. Williams, F. Ahmadpour, R. Clemmer, S. Tasnim, *J. Energy Storage* **2019**, *25*, 100844.
[11] L. Ye, S. Qi, T. Cheng, Y. Jiang, Z. Feng, M. Wang, Y. Liu, L. Dai, L. Wang, Z. He, *ACS Nano* **2024**, *18*, 18852.
[12] N. Poli, C. Bonaldo, M. Moretto, M. Guarnieri, *Appl. Energy* **2024**, *362*, 122954.
[13] N. T. Nassar, J. Brainard, A. Gulley, R. Manley, G. Matos, G. Lederer, L. R. Bird, D. Pineault, E. Alonso, J. Gambogi, S. M. Fortier, *Fed. Regist.* **2022**, *87*, 10381.
[14] K. E. Rodby, R. L. Jaffe, E. A. Olivetti, F. R. Brushett, *J. Power Sources* **2023**, *560*, 232605.
[15] Z. Huan, C. Sun, M. Ge, *WIREs Energy Environ.* **2024**, *13*, e541.
[16] Z. Li, T. Jiang, M. Ali, C. Wu, W. Chen, *Energy Storage Mater.* **2022**, *50*, 105.
[17] E. Sánchez-Díez, E. Ventosa, M. Guarnieri, A. Trovò, C. Flox, R. Marcilla, F. Soavi, P. Mazur, E. Aranzabe, R. Ferret, *J. Power Sources* **2021**, *481*, 228804.
[18] R. Rubio-Presa, L. Lubián, M. Borlaf, E. Ventosa, R. Sanz, *ACS Materials Lett.* **2023**, *5*, 798.
[19] E. Pedraza, C. de la Cruz, A. Mavrandonakis, E. Ventosa, R. Rubio-Presa, R. Sanz, S. T. Senthilkumar, P. Navalpotro, R. Marcilla, *Adv. Energy Mater.* **2023**, *13*, 2301929.
[20] C. Han, H. Li, R. Shi, T. Zhang, J. Tong, J. Li, B. Li, *J. Mater. Chem. A* **2019**, *7*, 23378.
[21] K. Lin, Q. Chen, M. R. Gerhardt, L. Tong, S. B. Kim, L. Eisenach, A. W. Valle, D. Hardee, R. G. Gordon, M. J. Aziz, M. P. Marshak, *Science* **2015**, *349*, 1529.
[22] H. Zhang, W. Lu, X. Li, *Electrochem. Energy Rev.* **2019**, *2*, 492.
[23] O. Nolte, I. A. Volodin, C. Stolze, M. D. Hager, U. S. Schubert, *Mater. Horiz.* **2021**, *8*, 1866.
[24] A. Clemente, M. Montiel, F. Barreras, A. Lozano, R. Costa-Castelló, *Electrochim. Acta* **2023**, *449*, 142117.
[25] X. Z. Yuan, C. Song, A. Platt, N. Zhao, H. Wang, H. Li, K. Fatih, D. Jang, *Int. J. Energy Res.* **2019**, *43*, 6599.
[26] T. J. Carney, S. J. Collins, J. S. Moore, F. R. Brushett, *Chem. Mater.* **2017**, *29*, 4801.
[27] L. Briot, M. Petit, Q. Cacciuttolo, M. C. Pera, *J. Power Sources* **2022**, *536*, 231427.
[28] M. Nourani, C. R. Dennison, X. Jin, F. Liu, E. Agar, *J. Electrochem. Soc.* **2019**, *166*, A3844.
[29] M. A. Goulet, L. Tong, D. A. Pollack, D. P. Tabor, S. A. Odom, A. Aspuru-Guzik, E. E. Kwan, R. G. Gordon, M. J. Aziz, *J. Am. Chem. Soc.* **2020**, *141*, 8014.
[30] Y. Jing, E. W. Zhao, M. A. Goulet, M. Bahari, E. M. Fell, S. Jin, A. Davoodi, E. Jónsson, M. Wu, C. P. Grey, R. G. Gordon, M. J. Aziz, *Nat. Chem.* **2022**, *14*, 1103.
[31] H. Li, Q. Zhu, Y. Dong, P. Zuo, Z. Yang, T. Xu, *J. Membr. Sci.* **2023**, *668*, 121195.
[32] K. Peng, C. Zhang, J. Fang, H. Cai, R. Ling, Y. Ma, G. Tang, P. Zuo, Z. Yang, T. Xu, *Angew. Chem. Int. Ed.* **2024**, *63*, e202407372.
[33] S. Lander, M. Vagin, V. Gueskine, J. Erlandsson, Y. Boissard, L. Korhonen, M. Berggren, L. Wågberg, X. Crispin, *Adv. Energy Sustainability Res.* **2022**, *3*, 2200016.
[34] T. Páez, A. Martínez-Cuezva, R. Marcilla, J. Palma, E. Ventosa, *J. Power Sources* **2021**, *512*, 230516.
[35] M. Cantera, L. Lubián, K. Cavusoglu, R. Rubio-Presa, R. Sanz, V. Ruiz, J. M. Cámara, E. Ventosa, *Batteries & Supercaps* **2024**, *7*, e202400086.
[36] S. Ressel, F. Bill, L. Holtz, N. Janshen, A. Chica, T. Flower, C. Weidlich, T. Struckmann, *J. Power Sources* **2018**, *378*, 776.
[37] Z. Wei, J. Zhao, D. Ji, K. J. Tseng, *Appl. Energy* **2017**, *204*, 1264.
[38] H. Wang, S. A. Pourmousavi, Y. Li, W. L. Soong, X. Zhang, B. Xiong, *J. Power Sources* **2024**, *603*, 234428.
[39] V. I. Vlasov, M. A. Pugach, D. S. Kopylova, A. V. Novikov, N. A. Gvozdik, A. A. Mkrtchyan, A. I. Davletkhanov, Y. G. Gladush, F. M. Ibanez, D. A. Gorin, K. J. Stevenson, *J. Power Sources* **2023**, *584*, 233600.
[40] T. Puleston, A. Cecilia, R. Costa-Castelló, M. Serra, *J. Energy Storage* **2023**, *68*, 107666.
[41] C. Stolze, P. Rohland, K. Zub, O. Nolte, M. D. Hager, U. S. Schubert, *Energy Convers. Manage.* **2022**, *14*, 100188.
[42] B. J. Neyhouse, K. M. Tenny, Y. M. Chiang, F. R. Brushett, *ACS Appl. Energ. Mater.* **2021**, *4*, 13830.

Manuscript received: November 16, 2024
Revised manuscript received: January 23, 2025
Accepted manuscript online: January 25, 2025
Version of record online: February 19, 2025